Journal of Hydrology 540 (2016) 96–105

Contents lists available at ScienceDirect

Journal of Hydrology

journal homepage: www.elsevier.com/locate/jhydrol

Mapping mean total annual precipitation in Belgium, by investigating the scale of topographic control at the regional scale

J. Meersmans [a,*], K. Van Weverberg [b], S. De Baets [a], F. De Ridder [c], S.J. Palmer [a], B. van Wesemael [d], T.A. Quine [a]

[a] University of Exeter, College of Life and Environmental Science, Department of Geography, United Kingdom
[b] Met Office, Exeter, United Kingdom
[c] Energy Technology, EnergyVille/VITO, Mol, Belgium
[d] Université catholique de Louvain, Georges Lemaitre Center for Climate Research, Earth and Life Institute, Louvain-la-neuve, Belgium

ARTICLE INFO

Article history:
Received 2 August 2015
Received in revised form 28 April 2016
Accepted 5 June 2016
Available online 9 June 2016
This manuscript was handled by Konstantine P. Georgakakos, Editor-in-Chief, with the assistance of Alan Seed, Associate Editor

Keywords:
Precipitation
Interpolation
Weather circulation
Slope
Altitude
Topography

SUMMARY

Accurate precipitation maps are essential for ecological, environmental, element cycle and hydrological models that have a spatial output component. It is well known that topography has a major influence on the spatial distribution of precipitation and that increasing topographical complexity is associated with increased spatial heterogeneity in precipitation. This means that when mapping precipitation using classical interpolation techniques (e.g. regression, kriging, spline, inverse distance weighting, etc.), a climate measuring network with higher spatial density is needed in mountainous areas in order to obtain the same level of accuracy as compared to flatter regions. In this study, we present a mean total annual precipitation mapping technique that combines topographical information (i.e. elevation and slope orientation) with average total annual rain gauge data in order to overcome this problem. A unique feature of this paper is the identification of the scale at which topography influences the precipitation pattern as well as the direction of the dominant weather circulation. This method was applied for Belgium and surroundings and shows that the identification of the appropriate scale at which topographical obstacles impact precipitation is crucial in order to obtain reliable mean total annual precipitation maps. The dominant weather circulation is determined at 260°. Hence, this approach allows accurate mapping of mean annual precipitation patterns in regions characterized by rather high topographical complexity using a climate data network with a relatively low density and/or when more advanced precipitation measurement techniques, such as radar, aren't available, for example in the case of historical data.

1. Introduction

Precipitation is widely recognized as an important factor controlling environmental processes and therefore forms an essential input variable in many applications aimed at predicting or investigating these processes. Some of these applications, such as models predicting avalanches or landslides (Nolin and Daly, 2006; Van Den Eeckhaut et al., 2006) require both the temporal and spatial scale of the input precipitation fields to be very detailed. Other applications, in contrast, such as regional land use models, biogeochemical cycle models (e.g. carbon storage) or models of the co-evolution of mountain ranges and climate systems only require very detailed spatial scales, while fairly coarse monthly or even annual temporal scales are sufficient (e.g. Daly et al., 1993; Kittel et al., 1997; Roe and Baker, 2006; Milne et al., 2007; Meersmans et al., 2012).

Recent studies (e.g. Parsons and Foster, 2011) have suggested that the spatial variability of long-term average precipitation might be fairly large even at a within field/(sub)catchment level (resolution < 1 km), consequently questioning the use of anthropogenic radionuclide Cesium (^{137}Cs), i.e. globally deposited following atmospheric nuclear-bomb tests in the past (mainly 1950–1960s), as a proxy for erosion (Parsons and Foster, 2011). Hence, identification of the resolution at which topography influences the spatial distribution of precipitation will be essential to evaluate the validity of commonly used precipitation fallout related radionuclide proxies (such as ^{137}Cs) at the landscape scale. One of the main reasons for the very large spatial variability of precipitation is its strong dependence on the terrain altitude and steepness as well as the orientation of the slopes. The literature indicates that even low elevation macro-relief structures can exhibit a significant effect on surface

* Corresponding author. Tel.: +44 (0)1392 72 44 88; fax: +44 (0)1392 72 33 42.
E-mail address: j.meersmans@exeter.ac.uk (J. Meersmans).

http://dx.doi.org/10.1016/j.jhydrol.2016.06.013
0022-1694/

precipitation rates (e.g. Minder et al., 2008). An extensive review of the physical mechanisms leading to larger precipitation amounts over terrain has been given recently by for example Roe (2005) and Houze (2012). Houze (2012) describes at least two distinct mechanisms that could lead a pre-existing frontal cloud to be enhanced and produce a precipitation maximum on the upwind side of a low barrier. Firstly, the terrain could facilitate the gradual rise of warm air ahead of frontal systems, while at the lee side of the hill the precipitating capacity is weakened by the down-slope air motion (Houze, 2012). Secondly, the feeder-seeder mechanism could enhance precipitation rates onto a ridge. In this case, an upper-level cloud (the feeder) is producing precipitation, while a low, shallow, orographically-induced cloud (the seeder) could act to enhance the precipitation by accretion of the cloud droplets onto the precipitating particles from the cloud above. During summer, convective events also contribute significantly to the total rainfall in the region of interest (Roe, 2005). Convective events might be affected by low terrain in various ways, e.g. by triggering by lee-waves in the wake of a hill (Houze, 2012). By the mechanism listed above, low elevation barriers do have the potential to influence the dominant weather circulation and, therefore, could exercise a primary control on the regional spatial precipitation pattern in these environments.

Despite the widely recognized importance of the spatial distribution of precipitation over complex terrain, many regional climate inventories are based on long term observations from sparse meteorological stations. For example, relatively coarse precipitation maps are available at the national or continental scale, from the ATEAM project (Mitchell et al., 2004). Most often, point data are extrapolated to a continuous grid by using classical interpolation techniques, such as nearest neighbor methods, local linear regression, inverse distance weighting, spline or kriging methods (without or with external drift) (e.g. Goovaerts, 2000; Lloyd, 2005; Daly, 2006; Basistha et al., 2008; Tobin et al., 2011). In most cases these techniques are not satisfactory, since the spatial heterogeneity of precipitation and their resolutions are sub-optimal for ecological and environmental modeling. Mapping precipitation in regions characterized by complex topography, such as mountainous regions, demands higher density measurements in order to obtain a climate map with a spatially uniform quality level when using classical interpolation techniques (Daly, 2006). Nevertheless, the cost of monitoring at sufficient density may be prohibitive and there is, therefore, a need to develop strategies for interpolation of data that capture the structure of precipitation patterns, which will help in setting-up more efficient monitoring networks.

This has lead over the last decades to increased efforts in developing techniques to obtain a more accurate interpolation, based on elevation data (e.g. Sen and Habib, 2000; Lloyd, 2005; Di Luzio et al., 2008; Gottardi et al., 2012) or using the slope orientation of mountain ranges (e.g. Turner et al., 2009; Hughes et al., 2008). One of the most promising approaches to the characterization of topographic control on spatial patterns of precipitation is the Precipitation-elevation Regressions on Independent Slopes Model (PRISM) (e.g. Daly et al., 2002). In this model precipitation is interpolated for each grid cell of the digital elevation model (DEM) based on a simple weighted precipitation-elevation regression with distance to station, coastal proximity, general slope orientation and vertical layer (inversion layer or not) as weighting factors. In the application of PRISM, it is critical to understand at which scale precipitation is influenced by the topography. Daly et al. (2002) explored this question using 6 DEMs with a differing smoothing level, based on station data density and local terrain complexity.

Even more advanced techniques combine information obtained from weather radar with that from rain gauges. Goudenhoofdt and Delobbe (2009) showed that a recent technique based on the geostatistical merging of weather radar and rain gauges provides spatially and temporally accurate daily rainfall accumulation predictions. While this approach certainly has the potential to improve our understanding of the relation between topography and precipitation, the fairly recent advent of weather radars prohibits the application of this approach to historical data, long time periods or regions not covered by weather radar.

Hence, there is still a need for interpolation techniques of intermediate complexity to obtain reasonable estimates of surface precipitation with high spatial resolution, only based on information from rain gauges and terrain characteristics. One of the main caveats with techniques like PRISM, is that it is not known a priori what the optimal scale is of the input fields. In addition, information on the prevailing rain-bearing wind direction could be a significant improvement to PRISM. To overcome this shortcoming, recently Gottardi et al. (2012) conducted a novel methodology to map daily precipitation amounts in main mountain ranges in France (i.e. Pyrenees, Central Massif and Alps) by combining a local elevation–precipitation model (comparable to PRISM) with a weather pattern classification. They defined 8 different weather patterns (e.g. Southwest circulation or anticyclonic) and an associated linear orographic precipitation gradient. The gridded precipitation was a function not only of elevation, but also of the weather-pattern specific gradient, giving weights to neighboring stations using a "crossing distance" and taking into account crests and valleys between the stations and the grid cell of interest. While this method provides very detailed daily estimates of surface precipitation, it is also computationally expensive, given the identification of the weather pattern for each day.

This study discusses a novel, computationally affordable interpolation technique, using the dominant rain-bearing wind direction and the optimal scales of topographical variables, aimed specifically at regions with sparse data over terrain with intermediate complexity or to reconstruct very detailed historical precipitation maps. The scale at which relief influences precipitation will be investigated, and the direction of the dominant weather circulation identified. These two components form essential elements in the present novel spatial precipitation model approach, which will help us to support the hypothesis of the existence of a rain shadow effect in these environments. More specifically, this methodological framework will be applied to a specific case study, i.e. predicting average yearly precipitation (1960–1990) in Belgium and surroundings, including the Ardennes–Eifel massif situated at the Belgian–German border (Fig. 1).

2. Material and methods

2.1. Study area

The northern and western parts of Belgium are situated in the North-west European lowlands and are characterized mainly by altitudes less than 100 m above sea level. The Ardennes–Eiffel massif covers the eastern and southern part of the study area and reaches altitudes up to 700 m (Fig. 1A). The study area is characterized by a temperate maritime climate, with a mean annual temperature and total annual precipitation amounts ranging from about 10 °C and 700 mm in the west to about 6 °C and 1400 mm in the southeast.

Fig. 1B shows that the 30-year average annual precipitation amounts of the stations in Kall (860 mm yr^{-1}) and Nuerburg (872 mm yr^{-1}), situated in the eastern part of the Ardennes – Eiffel massif at altitudes of respectively 550 and 629 m asl, are remarkably low compared to the stations near the summit and/or situated on the western part at similar or even lower altitudes (e.g. La

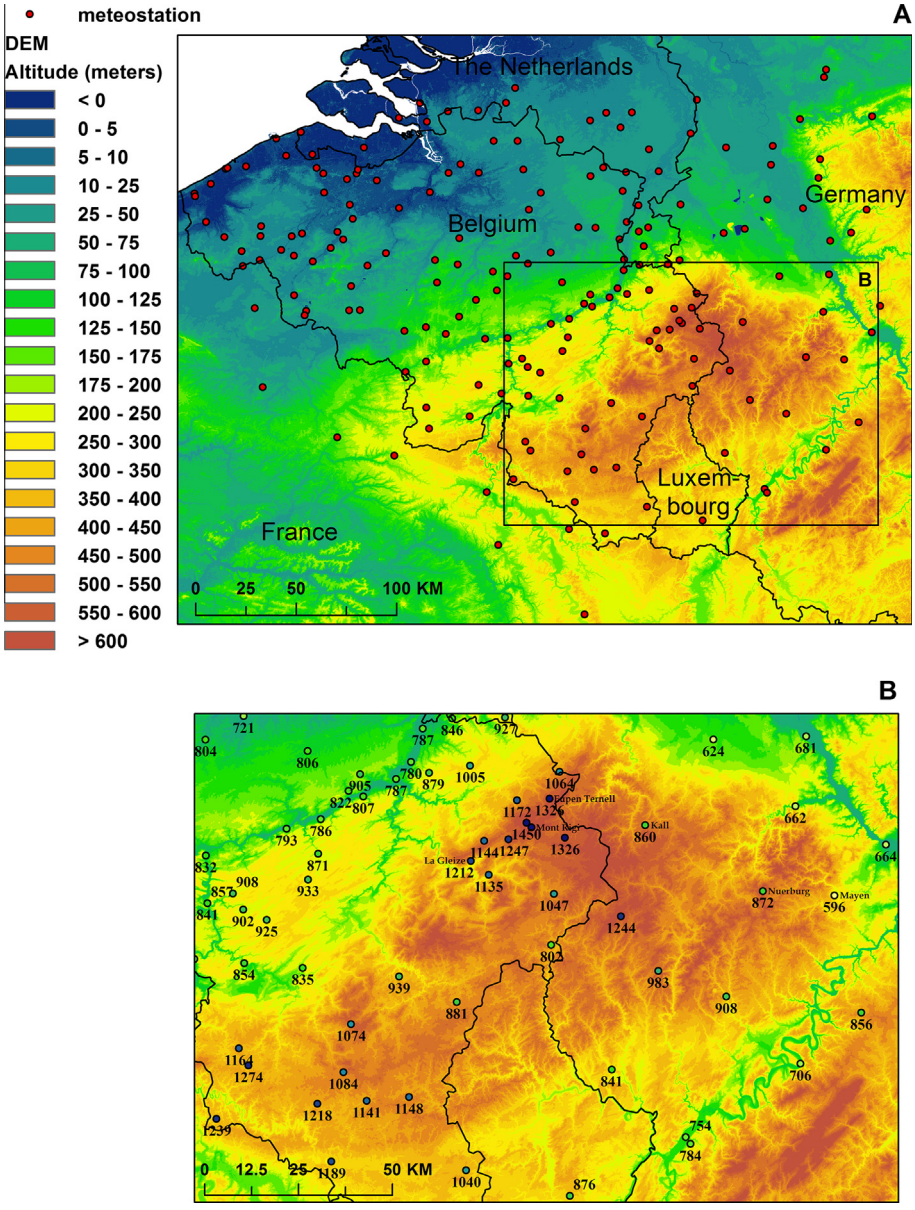

Fig. 1. (A) Localization of the 197 selected meteostations on the SRTM-DEM with a resolution of 90 m in and around Belgium. (B) Annotation of the measured 30-year average annual precipitation amounts (mm yr^{-1}) of the local meteostations along the Ardennes–Eiffel massif.

Gleize: 1212 mm yr^{-1} at 412 m asl, Eupen Ternell: 1326 mm yr^{-1} at 565 m asl, Mont Rigi: 1450 mm yr^{-1} at 680 m asl). Furthermore, the 30-year average annual precipitation amount in Mayen (230 m asl.) at 596 mm yr^{-1} is remarkably low. This station is situated in the most eastern part of the Ardennes–Eiffel massif and so probably very well shielded from east–west precipitation supply by the configuration of the mountain range. This clearly shows the existence of a rain shadow effect.

2.2. Climate and topographical data

Mean long-term climate data for the period 1961–1990 were obtained for Belgian stations from the 'Koninklijk Meteorologisch Instituut (KMI)', for the Southern part of The Netherlands from the 'Koninklijk Nederlands Meteorologisch Instuut (KNMI)', for West Germany from the 'Deutscher Wetterdienst (DWD)' and for North France from 'Meteo France'. In total 201 meteorological stations, with a good geographical spread, were selected for the analysis (Fig. 1A).

The "SRTM Digital Elevation Data" distributed by "The CGIAR Consortium for Spatial Information (CGIAR-CSI)" with a resolution of 90 m and produced by the NASA originally, were used as topographical source data (The CGIAR Consortium for Spatial Information, 2008).

2.3. Precipitation model

'Altitude' and 'deviation of the orientation of the slope to the orientation of the dominant weather circulation' were selected as input variables for the model. The orientation of the dominant rain-bearing weather circulation in the study area is from the west, as shown by e.g. Brisson et al. (2011). This is because all vast water bodies (i.e. North Sea and Atlantic Ocean) are situated in the west, and hence the dominant westerly winds at this latitude advect relative humid maritime air. This implies that under this assumption the 'deviation of the orientation of the slope to the ODWC' will express the angle between the west and the orientation of the slope. So under the assumption that west is the direction of the

dominant weather circulation, the more the slope orientation deviates from the west, the higher this value will be. For example, north and south oriented slopes are characterized by a value of 90°, while east oriented slopes have a value of 180°.

Moreover, we note that the influence of slope orientation on precipitation strongly depends on its altitude above sea level. For example, seawards oriented slopes can influence the weather circulation more efficiently when they are situated at higher altitude. Consequently, the 'deviation of the orientation of the slope to the ODWC' variable is expressed in the final model as an interaction term with altitude (Eq. (1)).

$$\text{prec} = a \cdot H_1 + b \cdot H_2 \cdot S + c \quad (1)$$

where

prec = long term (30 yrs) average annual precipitation amount (mm yr^{-1})
H_1 = height above sea level (m)
H_2 = height above sea level (m) in the interaction term
S = deviation of the orientation of the slope to the direction of the dominant weather circulation (ODWC)
a, b, c = model parameters

Note that the present model has been calibrated based on the 30-year average annual precipitation amounts from the 201 meteorological stations, but subsequently, this calibrated model has been applied in a spatial explicit way in order to obtain a precipitation map covering the entire study area. Moreover, although the H_1 and H_2 variables in this model both represents the height above sea level (either as a separate term or embedded in an interaction term), the associated values will most probably be different as they can be abstract from different levels of topographical detail as obtained after applying the present topographical smoothing procedure (see Section 2.4 and Fig. 2 for more details).

2.4. Detection of the scale of topographical control and orientation of the dominant weather circulation

As this study aims to detect the scale at which low elevation topographical barriers within the study area impact the spatial distribution of mean total annual precipitation, the present model's (Eq. (1)) performance was investigated using a wide range of input variable maps (H_1, H_2, S), reflecting different degrees of spatial heterogeneity. This allowed us to identify the optimal level of topographical detail of these variables in order to map mean total annual precipitation over the entire study area. In addition, the detection of the ODWC is another important element in the present methodology. Hence, the above made assumption of west as ODWC will be tested and refined if needed. A detailed description of the associated methodological approach can be found below, and a schematic overview is provided in Fig. 2.

After converting the original DEM into maps presenting the deviation of the slope toward 19 different potential ODWCs, i.e. every 10° between South (180°) and North (360°), the model's topographical input maps (H_1, H_2, S) were aggregated to different spatial resolutions. In total, 80 different levels of aggregation were considered, resulting in a set of maps ranging in resolution from 90 m to 103.5 km for each of the input variables. The resulting aggregated input maps were smoothed to remove unrealistically sharp gradients before running the model and producing spatial predictions. While all model input maps were resampled to a resolution of 90 m during the smoothing procedure, it is important to note that the same level of detail is maintained (i.e. determined by the aggregated map prior to smoothing). This allowed us to use continuous input maps and therefore make more realistic spatial model predictions. After comparing the performance of two commonly used interpolation techniques (i.e. "Spline" and "Natural Neighbor", e.g. Lam (1983)) for both "Altitude" and "Deviation of the orientation of the slope toward the West", our analysis led us to use "Spline" to smooth H_1 and H_2 and "Natural Neighbor" to smooth S model input maps (Fig. 3). For each of the 9,728,000 combinations of smoothed H_1, H_2 and S input maps, corresponding topographical values for all the meteo-stations were derived from the maps and the model (Eq. (1)) was applied to estimate 30-year average annual precipitation amounts (mm yr^{-1}).

For each potential ODWC, a combination of the H_1, H_2 and S maps with the highest determination coefficient (R^2), was selected and compared to detect a more accurate ODWC. The finally selected model output (i.e. with the overall highest R^2) was combined with associated H_1, H_2 and S maps at corresponding resolutions in order to produce a 30-year average annual precipitation (mm yr^{-1}) map for Belgium.

2.5. Cross validation

In addition, for every potential ODWC, a repeated 10-fold cross validation procedure was carried out (1000 replicates) on each best model fit (i.e. map resolutions with highest R^2). Thereby, 90% of the data was randomly chosen for calibration and 10% for validation as it is commonly recommended (Hastie et al., 2001). By comparing the predicted and observed values of the validation samples Root Mean Square Error (RMSE, Eq. (2)) and Ratio of Performance to Deviation (RPD, Eq. (3)) of the model were calculated. The latter expresses how many times the predictive ability of the model is stronger than just using the average precipitation value. In other

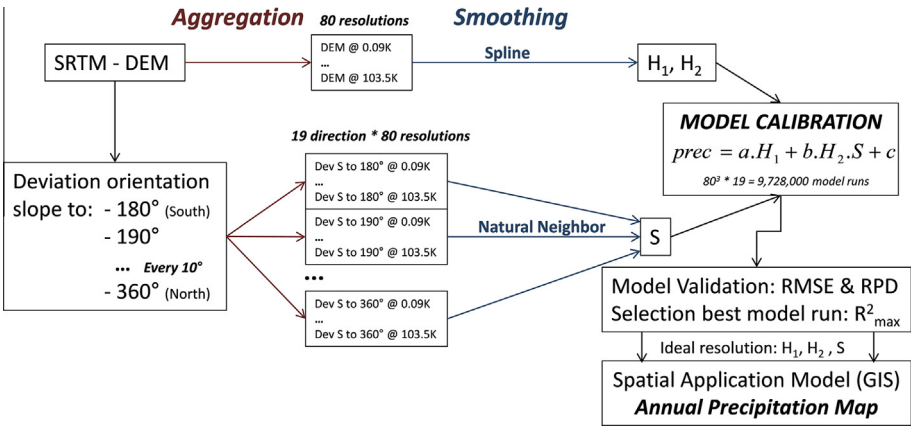

Fig. 2. Methodological flowchart.

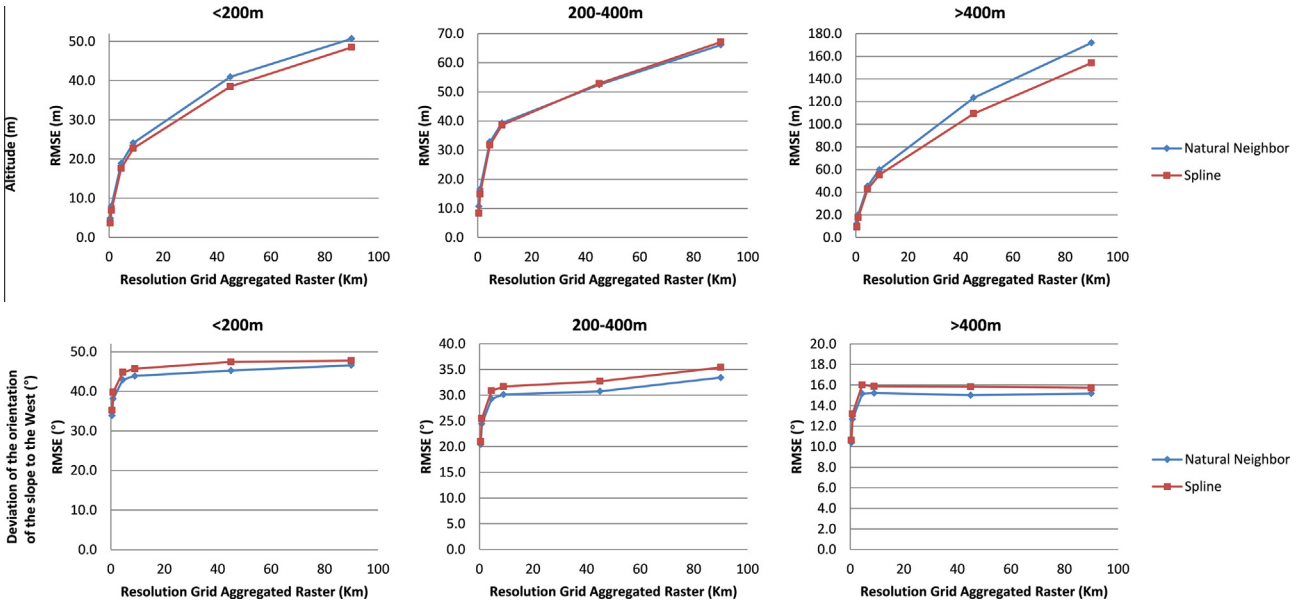

Fig. 3. Comparison of interpolation techniques "Spline" and "Natural Neighbor" used to smooth aggregated model input maps of Altitude and "Deviation to the orientation of the slope to the West" at 3 different altitude intervals (<200 m, 200–400 m, >400 m).

words, RPD values of 2, 3 and 4 mean that respectively 50%, 66.67% and 75% of the total variation in the validation dataset is captured by the model.

$$\mathrm{RMSE} = \sqrt{\frac{1}{n} \cdot \sum_{i=1}^{n} \left(P_{obs(i)} - P_{pred(i)}\right)^2} \quad (2)$$

where RMSE is Root Mean Square Error (mm yr^{-1}), n is overall number of samples used in the validation procedure, $P_{obs(i)}$ is the observed value of *i*th 30-year average annual precipitation measurement (mm yr^{-1}) and $P_{pred(i)}$ is the predicted value of *i*th 30-year average annual precipitation measurement (mm yr^{-1}).

$$\mathrm{RPD} = \frac{\mathrm{STD}}{\mathrm{RMSE}} \quad (3)$$

With RPD being the ratio of performance to deviation and STD is standard deviation of all total yearly precipitation measurements (mm yr^{-1}).

3. Results and discussion

3.1. Topographical smoothing

In Fig. 3 the performances of the interpolation techniques "Spline" and "Natural Neighbor" in order to smooth "altitude" and "deviation of the orientation of the slope to the West" maps were analyzed. This was based on RMSE-output obtained by comparing the basic topographical data (i.e. SRTM-DEM derived) at a resolution of 90 m with a range of smoothed maps, i.e. at corresponding aggregation resolution levels of 0.45 km, 0.9 km, 4.5 km, 9 km, 45 km, 90 km, considering 3 different height classes (i.e. <200 m; 200–400 m and >400 m). These results show that Spline is the best interpolation method when smoothing the altitude (H_1, H_2, Eq. (1)) maps (i.e. lowest RMSE), at least when considering height classes <200 m and >400 m. No clear differences have been found for the 200–400 m height class. On the contrary, when considering the "deviation of the orientation of the slope to the West" Natural Neighbor seems to be the best interpolation method, with lower RMSE values than Spline for all altitude classes. Moreover, it's important to note that Spline returns values out of the theoretical possible range of 0–180°, which is an additional reason why Natural Neighbor is the most appropriate interpolation technique to be used when smoothing the "deviation of the orientation of the slope to the ODWC" (*S*, Eq. (1)) maps.

3.2. Model parameter identification and performance

Table 2 shows that the best model fit, i.e. with highest R^2, was obtained using the smoothed altitude maps derived from aggregated DEMs with a resolution of 8.1 and 90 km, for respectively H_1 and H_2 (Eq. (1)), and a "deviation of the orientation of the slope to 260° (i.e. the orientation of the dominant weather circulation, ODWC) map" with a resolution of 30.6 km. This model fit has an R^2 value of 0.82 and all estimated parameters are significant ($p < 0.05$) (Table 1). Table 2 shows an overview of the top 10 of best model fits, ranked based on R^2, with annotation of ODWC and aggregation resolution of smoothed model input maps (H_1, H_2 and S (Eq. (1))). It is remarkable that within this top 10 of best model runs (with R^2 values ranging between 0.8149 and 0.8192), there is only limited variation in ODWC and aggregation resolution of smoothed model input maps. For example besides 6 model fits with an ODWC of 260°, 4 model fits have an ODWC of 270°, which may suggest that more precisely the ODWC is situated somewhere in between 260° and 270°. Fig. 4 shows the determination coefficients of the different model runs as function of the aggregation resolution of the smoothed DEM (H_1 and H_2) and S maps including the selected best model run at $R^2 = 0.82$. The trendlines in these figures are a combination of a power and exponential law. It is interesting to note that for variable H_1, an additional linear term was required to fit the distribution, especially the very low R^2 values at lower resolutions, indicating the importance of the term of vari-

Table 1
Estimated parameter values of the selected model (i.e. resolution of H_1 = 8.1 km, H_2 = 90 km, S = 30.6 km, and orientation of dominant weather circulation (ODWC) of 260°).

Parameter	Value	95% confidence interval	
a	1.3309	1.4269	1.2348
b	−0.0115	−0.0100	−0.0130
c	777.16	790.73	763.59

Table 2
Top 10 best model runs ranked following R^2 with annotation of the "Orientation of the dominant weather circulation" (ODWC) and aggregation resolution of smoothed model input maps (H_1, H_2 and S (Eq. (1))).

Rank	R^2	ODWC (°)	Resolution		
			H_1 (km)	H_2 (km)	S (km)
1	0.8192	260	8.1	90.0	30.6
2	0.8187	260	8.1	90.0	27.0
3	0.8186	270	8.1	94.5	27.0
4	0.8181	260	8.1	94.5	30.6
5	0.8179	270	8.1	94.5	30.6
6	0.8178	260	8.1	94.5	27.0
7	0.8155	270	8.1	99.0	27.0
8	0.8155	260	8.1	68.4	30.6
9	0.8154	260	7.2	90.0	30.6
10	0.8149	270	7.2	94.5	30.6

able H_1 in the model as well as the selection of the appropriate level of spatial detail of these variables. Despite the fact that 8.1 km has been identified as the most appropriate aggregation resolution of H_1 input maps, the trendline (reaching its max. value at a resolution of 4.5 km) indicates that using an H_1 map with a finer resolution (i.e. within the 4–8 km resolution range) seems to be a valuable option as well (Fig. 4a). The range of potentially useful aggregation resolutions of maps representing the variables in the interaction factor is wider with roughly 50–100 km for H_2 (i.e. trendline's max. value at 70.8 km, Fig. 4b) and 20–40 km for S (i.e. trendline's max. value at 30.2 km, Fig. 4c). In addition the range of R^2 values covered by these variables (i.e. 0.64–0.82) shows that including the interaction factor in the model instead of simplified version whereby precipitation is only predicted as a linear function of altitude, results in a significant improvement of the R^2 with 0.18 (Fig. 4b and c). Moreover, the model cross-validation shows a root mean square error (RMSE) of 66.0 mm yr^{-1} and ratio of performance to deviation (RPD) of 2.33. Fig. 5 illustrates RMSE and RPD values of the H_1, H_2 and S maps combination with the maximal R^2 as a function of orientation of the dominant weather circulation. The results show that the selected best model fit has the best validation statistics, i.e. lowest RMSE and highest RPD, and underlines that the dominant weather circulation in Belgium is most probably at or very close to 260°.

The precipitation map we derived (Fig. 6) shows that precipitation increases with increasing altitude (Fig. 6). Furthermore, as this study detects a ODWC at an aspect of 260° for the study area, the Ardennes–Eiffel massif is influenced by a mainly west–east oriented weather circulation, resulting in higher precipitation amounts at the western side of the Ardennes massif (Belgium) compared to the eastern side (Eiffel – Germany) (Fig. 6). To detect this effect one should consider the macro relief structure of the topographical barrier. These findings underline the importance of the influence of lower elevation relief units on the spatial distribution of precipitation patterns and clearly show orographic precipitation and the existence of a rain shadow effect, i.e. in this particular study, in the western and the eastern parts of the Ardennes–Eiffel massif, respectively. Furthermore, the model predicts that smaller topographical barriers (i.e. mostly north–south oriented relief units with dimensions between 10 and 50 km) have an influence on spatial distribution of precipitation as well, such as the north–south oriented cuestas in the North-east of France (A) and the plateau in the eastern part of Limburg (north-east Belgium, B) or as indicated by the higher precipitation values in the Condroz region (C) as compared to Fagne-Famenne depression (D) (Figs. 1 and 6).

In general, relative errors are restricted and in most areas to below 10% (Fig. 6). No clear dominant regional pattern error can be detected. Nevertheless most important relative errors are found in the western part of the Ardennes–Eifel massif, characterized by high precipitation amounts, with more precisely a clear local underprediction in the South – Southwest and Northwest (I) and an overprediction in central (II) parts of this particular region. Furthermore, one can observe a general tendency of overprediction east of the Eifel (i.e. Mosel and Rhine Valley (III), as well as in

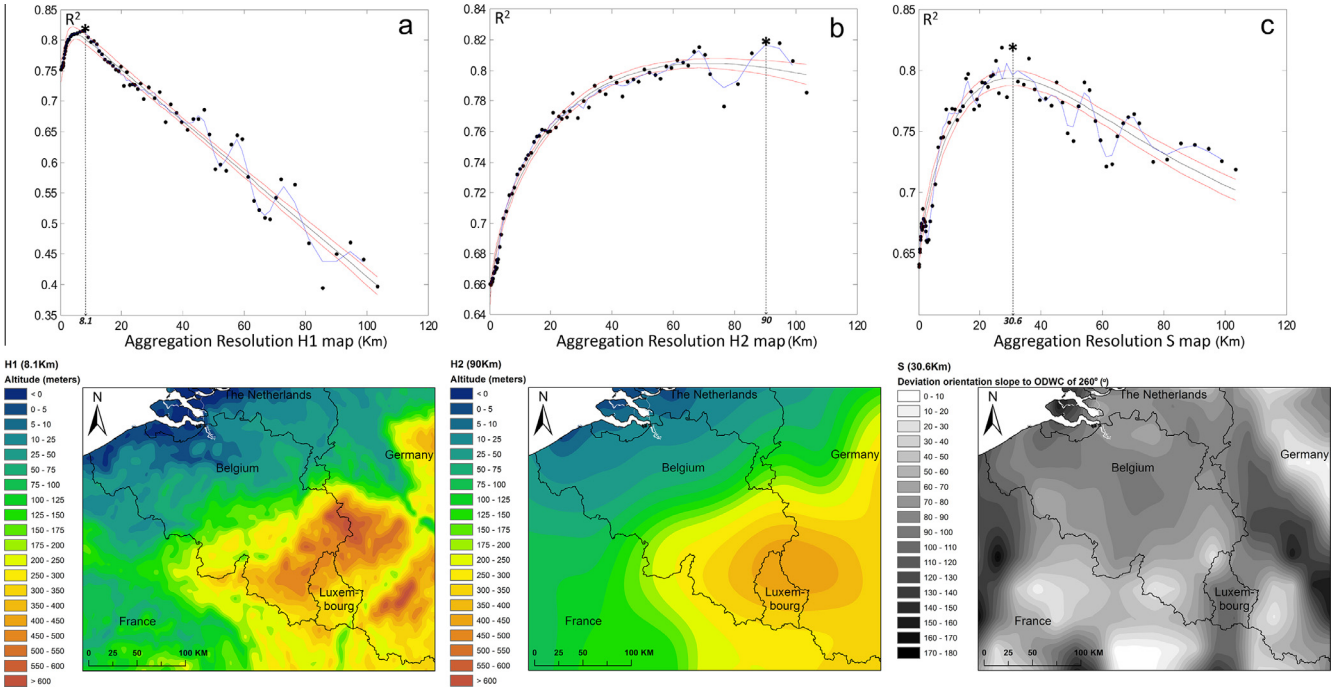

Fig. 4. Determination coefficients (R^2) of the different precipitation model runs as a function of the resolution of the aggregation level of the altitude input maps (km), i.e. (a) H_1 and (b) H_2 (Eq. (1)), and deviation of the orientation of the slope to the dominant weather circulation (260°) maps, i.e. (c) S (Eq. (1)), including the selected best model run as indicated by $*$ (R^2_{max} = 0.8192) as well as presentation of associated input maps (i.e. H_1 at 8.1 km; H_2 at 90 km and S at 30.6 km).

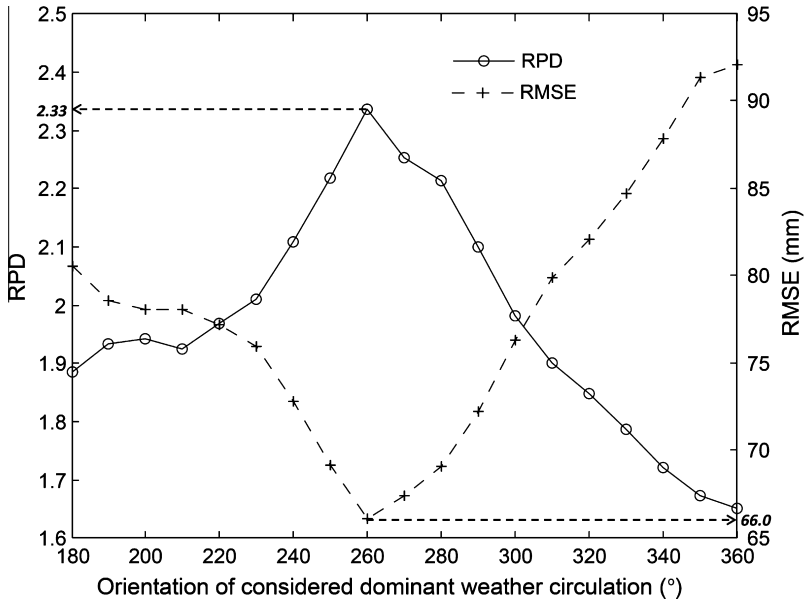

Fig. 5. Root Mean Square Error (RMSE, mm) and Ratio of Performance to Deviation (RPD) of the best model fit (R^2_{max}) in function of orientation of dominant weather circulation (°).

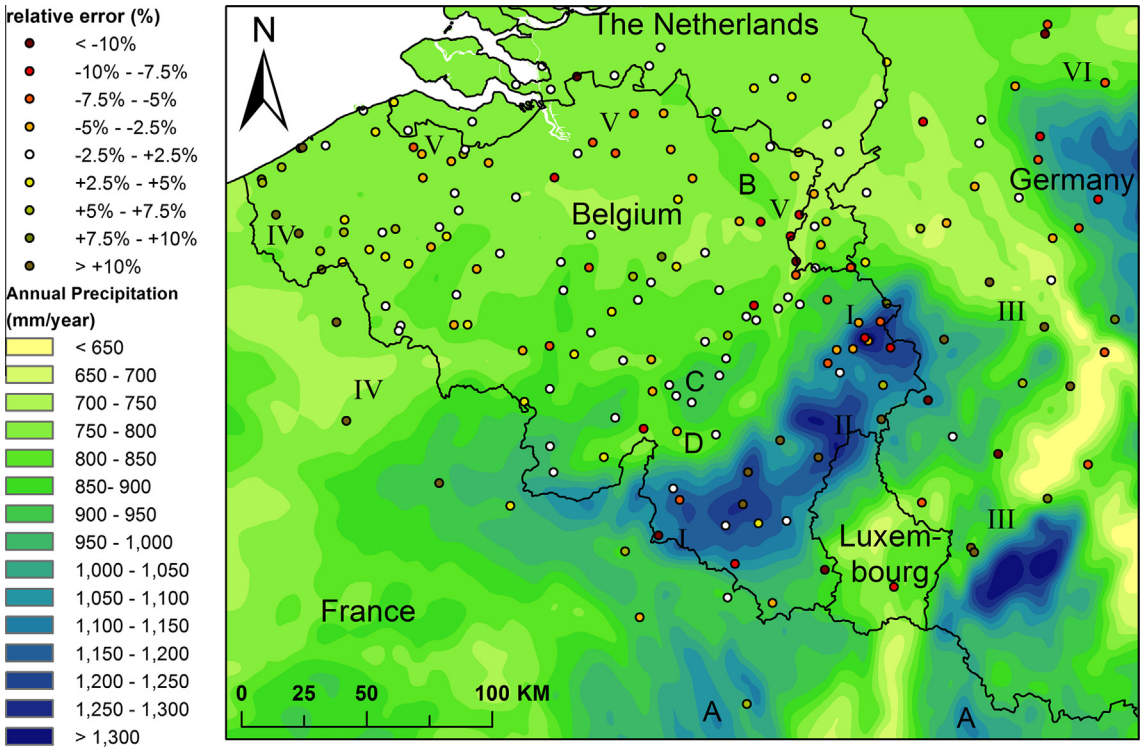

Fig. 6. Estimated long term (1960–1990) total 30-year average annual precipitation map (mm yr^{-1}) for Belgium and surroundings with indication of relative error (%) at meteo-stations.

the most western part of Belgium and Northwest of France (IV) and an underprediction in the North of Belgium (V) as well is in the Northeastern corner of the study area (VI) (Fig. 5).

The present precipitation mapping method answers two important questions:

(1) at which scale does topography influence the spatial pattern of precipitation? and

(2) what is the orientation of the dominant weather circulation (ODWC)?

In comparison to classical interpolation techniques, it allows accurate mapping in regions characterized by high topographical complexity without the need of a dense measuring network. Moreover, as the input data is restricted, i.e. a rather coarse DEM (e.g. SRTM 90 m covering entire world and free available) and climate

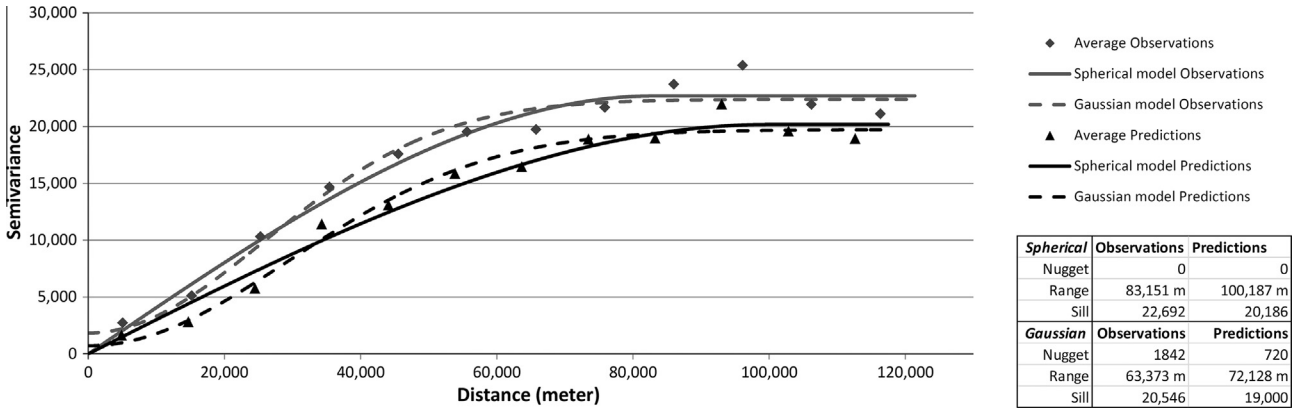

Spherical	Observations	Predictions
Nugget	0	0
Range	83,151 m	100,187 m
Sill	22,692	20,186
Gaussian	**Observations**	**Predictions**
Nugget	1842	720
Range	63,373 m	72,128 m
Sill	20,546	19,000

Fig. 7. Semivariograms of the observed data (gray) versus predicted precipitation values (black). The Spherical and Gaussian models as fitted through the averaged semivariance values and associated nugget, range and sill values are obtained by using ARC-GIS' Geostatistical Wizard tool.

data at common measurement density, we believe that the method has great potential to be applied in other regions characterized by a comparable topographical complexity in order to improve particular spatial prediction of the precipitation pattern. In addition, as the present method is based on a simple formula, it has the advantage of being a computationally 'low-cost' approach, increasing its applicability, especially as compared to other recently developed advanced precipitation interpolation methods (e.g. Gottardi et al., 2012) where for each spatial–temporal unit (pixel/day), a calibration procedure needs to be carried out. A simplified version of the present model (i.e. without ODWC detection component) has been recently applied successfully in a study conducting a spatial and temporal analysis of soil organic carbon in Belgium (Meersmans et al., 2011), underlining the need of detailed precipitation maps (and mapping methods) as essential input information for accurate spatial prediction of (soil) key environmental parameters. Furthermore, it is important to notice that the present methodology complements more advanced techniques, making use of radar and providing spatial information of precipitation at very fine spatial and temporal scales (Goudenhoofdt and Delobbe, 2009). This is especially relevant for regions with a high topographical complexity, but characterized by sparse climatological data network and/or when the aim is to map historical precipitation data (i.e. when radar was not yet available or for averages over longer periods in time). Finally, the fact that 8, 36 and 90 km are identified as the optimum scales at which topography influences precipitation (respectively for H_1, S and H_2 (see Eq. (1))), seems to reject Parsons and Foster's (2011) concern regarding the use of ^{137}Cs as a proxy for erosion due to a potential significant variation in fallout by precipitation at the within field scale (i.e. at resolutions below 1 km). Nevertheless, it should be stressed that we identified the optimal scales for the topography for this region specifically, and therefore, it is probable that these optimal scales might be different for other regions in the world characterized by different a degrees of terrain complexity or macro meteorological settings, such as more alpine environments.

3.3. Comparison against kriging

As previous studies have illustrated the high potential of using advanced geostatistical methods such as kriging to interpolate mean annual and seasonal precipitation amounts at the regional scale, underlining the importance of the existence of a significant spatial autocorrelation in the data (e.g. Dingman et al., 1988; Goovaerts, 2000; Masson and Frei, 2014), we have (i) evaluated if the predicted precipitation amounts obtained by the presented model preserved the spatial variability of the underlying observations; and (ii) made a comparison between the precipitation maps obtained with the model presented in this study and by applying Ordinary Kriging.

Fig. 7 compares the semivariograms, as produced by ARC-GIS' Geostatistical Wizard tool, from the observed data and the model predicted values. Although this figure shows that the average semivariance (see e.g. Goovaerts (2000) for equation) at any given distance between points is slightly lower in the case of the estimated values as compared to the original data, the nugget, range and sill are rather comparable considering both the Spherical and Gaussian model fits. When comparing predicted against observed values, the range is 20% and 15% higher, while the sill is 12% and 8% lower, for the Spherical and Gaussian model fits respectively (Fig. 7). These results indicate that the model output preserves to a large extent the spatial variability of the precipitation data.

The comparison of the spatial patterns in precipitation obtained by the approach presented in this study (Fig. 8A) with Ordinary Kriging (Fig. 8B), shows that Ordinary Kriging produces a much less detailed image in the more topographical complex zone in the Eastern part of the study area (i.e. along the Ardennes–Eifel massive) in comparison to the approach presented in this study (Fig. 8A and B). In contrast, in the Northern and Western parts of the study area, where no significant topographical features are present, Ordinary Kriging predicts a larger spatial variability in precipitation as compared to our approach (Fig. 8A and B). In addition, although the relative differences between both precipitation maps are generally larger than the relative model errors (bias) of the present approach (i.e. typically below 30% and 10%, respectively (Fig. 8C)), a spatial correlation exists between both. More precisely, precipitation values are generally higher for this study's modeled precipitation map compared to the map generated with Ordinary Kriging in areas in which the model is characterized by a regional overall trend of over-predictions (II, III & IV, Figs. 6 and 8C). In areas in which the model is characterized by a regional overall trend of under-prediction (I, V & VI Figs. 6 and 8C), precipitation values are considerably lower on this study's map compared to the map created by Ordinary Kriging. This indicates the largely complementary character of both methodologies, as it seems that Ordinary Kriging may have the potential to compensate for regional under/over predictions made by the presented model. Hence, one can conclude that there exists a scope for future research in which both interpolation methods could be combined in order to improve the overall performance of rainfall predictions in this or similar study areas. Another potential future avenue of research can be the application of the presented model at smaller temporal scales such as seasonal or monthly averaged total rainfall amounts.

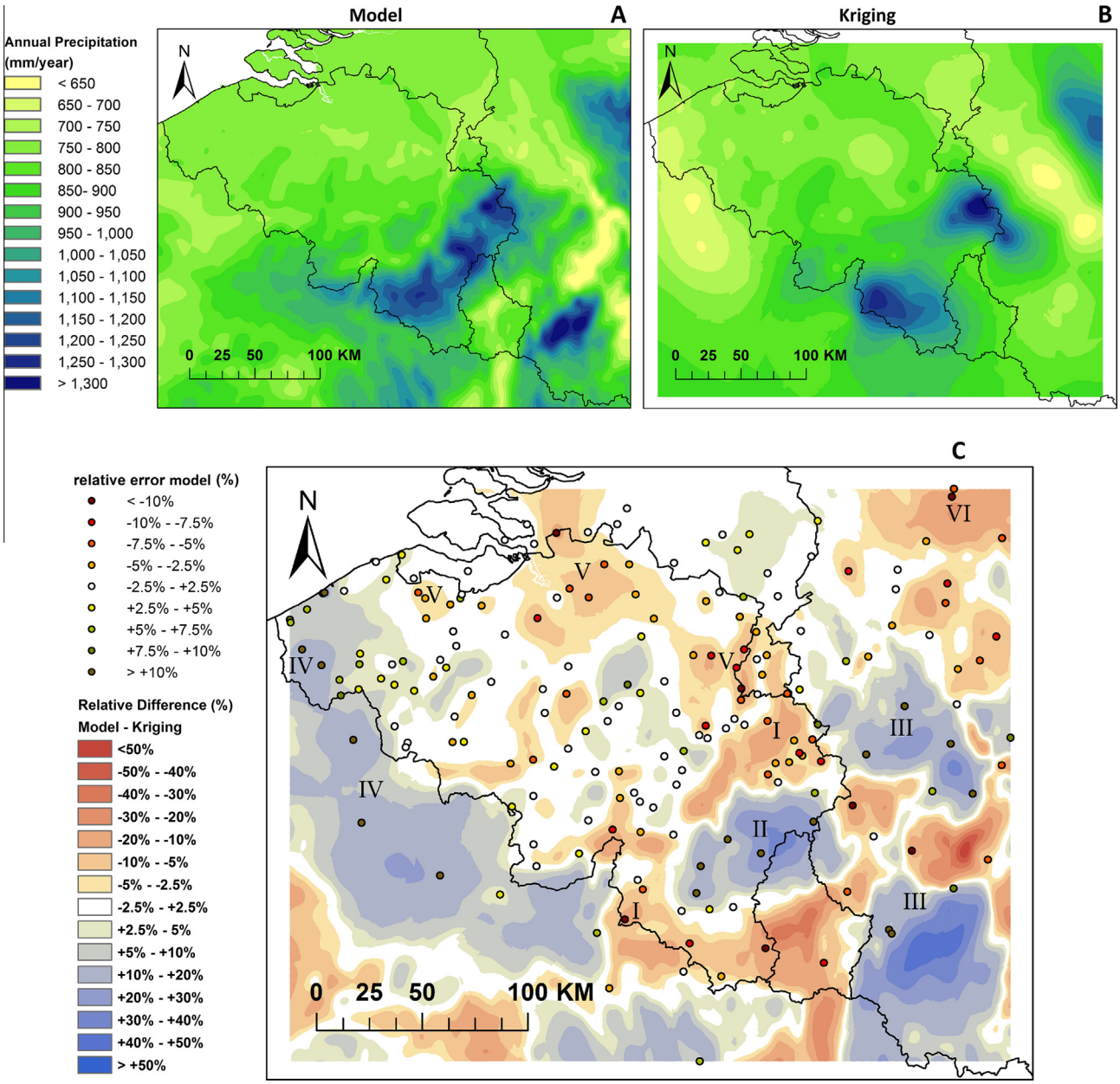

Fig. 8. Subpanel (A and B) are showing precipitation maps as obtained by the presented approach and the Ordinary Kriging, respectively. Subpanel (C) shows the relative difference between A and B, including the relative error of the model as presented in Fig. 6.

4. Conclusion

This study shows that long term mean annual precipitation amounts are strongly influenced by topography in lower elevation relief structures and offers a simple methodology to map climatologically averaged precipitation patterns in these regions when lacking a dense meteorological measuring network. Mean annual precipitation can be modeled as a function of smoothed altitude and slope orientation maps. Best results were obtained using smoothed altitude maps at aggregation resolutions of 8.1 km and 90 km (i.e. outside (H_1) and within interaction term (H_2) of the model (Eq. (1)), respectively) and a smoothed slope orientation map showing a deviation of the slope orientation to the north aspect of 260°, indicating the orientation of the dominant weather circulation (ODWR), at aggregation resolution of 30.6 km. The resulting precipitation map shows clearly that the Ardennes–Eiffel massif range determines, to a large extent, the spatial distribution of total yearly precipitation amount in the region. As this lower elevation relief units block precipitation supply from dominant west–east weather circulations, the western part of this topographical barrier receives remarkably higher precipitation amounts than the eastern side situated in the rain shadow of this mountain range. Furthermore, given the limited need for input data, this method is easily applicable to other regions. Hence, the method has a large potential to improve the interpolation of spatial patterns of precipitation in mountainous regions, characterized by a sparse data network and/or when more modern and advanced techniques, such as weather radars, are not available.

Acknowledgement

We are grateful to the National Meteorological Institutes of Belgium (Koninklijk Meteorologisch Instituut (KMI)), France (Meteo France), The Netherlands (Koninklijk Nederlands Meteorologisch

Instuut (KNMI)) and Germany (Deutscher Wetterdienst (DWD)) for providing the data. In addition we thank the two anonymous reviewers, whose comments resulted in significant improvements to the manuscript.

References

Basistha, A., Arya, D.S., Goel, N.K., 2008. Spatial distribution of rainfall in Indian Himalayas – a case study of Uttarakhand region. Water Resour. Manage 22, 1325–1346.

Brisson, E., Demuzere, M., Kwakernaak, B., van Lipzig, N.P.M., 2011. Relations between atmospheric circulation and precipitation in Belgium. Meteorol. Atmos. Phys. 111, 27–39.

Daly, C., Neilson, R.P., Philips, D.L., 1993. A statistical-topographical model for mapping climatological precipitation over mountainous terrain. J. Appl. Meteorol. 33, 140–158.

Daly, C., Wayne, G.P., Taylor, G.H., Johnson, G.L., Pasteris, P., 2002. A knowledge-based approach to the statistical mapping of climate. Climate Res. 22, 99–103.

Daly, C., 2006. Guidelines for assessing the suitability of spatial climate data sets. Int. J. Climatol. 26, 707–721.

Di Luzio, M., Johnson, G.L., Daly, C., Eischeid, J.K., Arnold, J.G., 2008. Constructing retrospective gridded daily precipitation and temperature datasets for the conterminous United States. J. Appl. Meteorol. Climatol. 47, 475–497.

Dingman, S.L., Seely-Reynolds, D.M., Reynolds, R.C., 1988. Applications of kriging to estimating mean annual precipitation in a region of orographic influence. Water Resour. Bull. 24, 329–339.

Goovaerts, P., 2000. Geostatistical approaches for incorporating elevation into the spatial interpolation of rainfall. J. Hydrol. 228, 113–129.

Gottardi, F., Obled, C., Gailhard, J., Paquet, E., 2012. Statistical reanalysis of precipitation fields based on ground network data and weather patterns. Applications over French mountains. J. Hydrol. 432–433, 154–167.

Goudenhoofdt, E., Delobbe, L., 2009. Evaluation of radar-gauge merging methods for precipitation estimates. Hydrol. Earth Syst. Sci. 13, 195–203.

Hastie, T., Tibshirani, R., Friedman, J., 2001. The Elements of Statistical Learning, Data Mining, Inference, and Prediction, Springer Series in Statistics, second ed. Springer-Verlag, New York.

Houze, R.A., 2012. Orographic effects on precipitating clouds. Rev. Geophys. 50. http://dx.doi.org/10.1029/2011RG000365.

Hughes, M., Hall, A., Fovell, R.G., 2008. Blocking in areas of complex topography, and its influence on rainfall distribution. J. Atmos. Sci. 66, 508–518.

Kittel, T.G.F., Royle, J.A., Daly, C., Rosenbloom, N.A., Gibson, W.P., Fisher, H.H., Schimel, D.S., Berliner, L.M., 1997. A gridded historical (1985–1993) bioclimate dataset for the conterminous United States. In: 10th Conference on Applied Climatology, pp. 219–222.

Lam, N.S.-N., 1983. Spatial interpolation methods: a review. Am. Cartographer 10, 129–150.

Lloyd, C.D., 2005. Assessing the effect of integrating elevation data into the estimation of monthly precipitation in Great Britain. J. Hydrol. 308, 128–150.

Masson, D., Frei, C., 2014. Spatial analysis of precipitation in a high-mountain region: exploring methods with multi-scale topographic predictors and circulation types. Hydrol. Earth Syst. Sci. 18, 4543–4563.

Minder, R.J., Durran, D.R., Roe, G.H., Anders, A.M., 2008. The climatology of small-scale orographic precipitation over the Olympic Mountains: patterns and processes. Q. J. R. Meteorol. Soc. 134, 817–839.

Milne, E., Al Adamat, R., Batjes, N.H., Bernoux, M., Bhattacharyya, T., Cerri, C.C., Cerri, C.E.P., Coleman, K., Easter, M., Falloon, P., Feller, C., Gicheru, P., Kamoni, P., Killian, K., Pal, D.K., Paustian, K., Powlson, D.S., Rawajfih, Z., Sessay, M., Williams, S., Wokabi, S., 2007. National and sub-national assessments of soil organic carbon stocks and changes: the GEFSOC modelling system. Agric. Ecosyst. Environ. 122, 3–12.

Mitchell, T.D., Carter, T.R., Jones, P.D., Hulme, M., New, M., 2004. A comprehensive set of high resolution grids of monthly climate for Europe and the globe: the observed record (1901–2000) and 16 scenarios (2001–2100). Tyndall Centre working Paper, vol. 55. University of East Anglia, Norwich, United Kingdom.

Meersmans, J., van Wesemael, B., Goidts, E., Van Molle, M., 2011. Spatial analysis of soil organic carbon evolution in Belgian croplands and grasslands, 1960–2006. Glob. Change Biol. 17, 466–479.

Meersmans, J., Martin, M.P., Lacarce, E., De Baets, S., Jolivet, C., Boulonne, L., Lehmann, S., Saby, N.P.A., Bispo, A., Arrouays, D., 2012. A high resolution map of French soil organic carbon. Agronomy Sustain. Dev. 32, 841–851.

Nolin, A., Daly, C., 2006. Mapping "At Risk" snow in the pacific northwest. J. Hydrometeorol. 7, 1164–1171.

Parsons, A.J., Foster, I.D.L., 2011. What can we learn about soil erosion from the use of ^{137}Cs? Earth Sci. Rev. 108, 101–113.

Roe, G.H., 2005. Orographic precipitation. Annu. Rev. Earth Planet. Sci. 33, 645–671.

Roe, G.H., Baker, M.B., 2006. Microphysical and geometrical controls on the pattern of orographic precipitation. Am. Meteorol. Soc. 63, 861–880.

Sen, Z., Habib, Z., 2000. Spatial precipitation assessment with elevation by using point cumulative semivariogram techniques. Water Resour. Manage 14, 311–325.

The CGIAR Consortium for Spatial Information, 2008. SRTM Digital Elevation Data. <http://srtm.csi.cgiar.org/>.

Tobin, C., Nicotina, L., Parlange, M.B., Berne, A., Rinaldo, A., 2011. Improves interpolation of meteorological forcings for hydrologic applications in a Swiss Alpine region. J. Hydrol. 401, 77–89.

Turner, J., Connolley, W.M., Leonard, S., Marshall, G.J., Vaughan, D.G., 2009. Spatial and temporal variability of net snow accumulation over the Antarctic from ECMWF re-analysis project data. Int. J. Climatol. 19, 697–724.

Van Den Eeckhaut, M., Vanwalleghem, T., Poesen, J., Govers, G., Verstraeten, G., Vandekerckhove, L., 2006. Prediction of landslide susceptibility using rare events logistic regression: a case-study in the Flemish Ardennes, Belgium. Geomorphology 76, 392–410.